

# Computation-Efficient and Recognition-Friendly 3D Point Cloud Privacy Protection

Haotian Ma

hxm3470@mavs.uta.edu

Lin Gu

lin.gu@riken.jp

Siyi Wu

sxw8121@mavs.uta.edu

Yingying Zhu

yingying.zhu@uta.edu

## Abstract

3D point cloud has been widely used in applications such as self-driving cars, robotics, CAD models, etc. To the best of our knowledge, these applications raised the issue of privacy leakage in 3D point clouds, which has not been studied well. Different from the 2D image privacy, which is related to texture and 2D geometric structure, the 3D point cloud is texture-less and only relevant to 3D geometric structure. In this work, we defined the 3D point cloud privacy problem and proposed an efficient privacy-preserving framework named *PointFlowGMM* that can support downstream classification and segmentation tasks without seeing the original data. Using a flow-based generative model, the point cloud is projected into a latent Gaussian mixture distributed subspace. We further designed a novel angular similarity loss to obfuscate the original geometric structure and reduce the model size from 767MB to 120MB without a decrease in recognition performance. The projected point cloud in the latent space is orthogonally rotated randomly to further protect the original geometric structure, thus, the protected point cloud can support the recognition task. We evaluated our model on multiple datasets and achieved comparable recognition results on encrypted point clouds compared to the original point clouds.

## 1. Introduction

The rapid development of sensor devices such as LiDAR [20], as well as advances in technologies such as augmented reality (AR), mixed reality (MR) and self-driving cars, have greatly facilitated three-dimensional (3D) point cloud research from classification [33], segmentation [29], localization [13], vehicle positioning [15, 25], CAD model [12, 28], etc. However, these 3D vision systems also pose significant privacy threats to the public[4, 9].

As shown in Figure 1, the privacy of 2D images and videos has been extensively researched in computer vision. Approaches to protect 2D-related data include replacing or removing sensitive features[1, 3, 8, 11, 16],

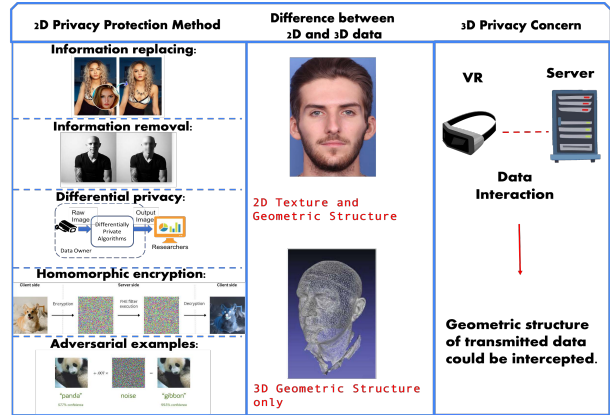


Figure 1. On the left side, various 2D privacy-preserving techniques are shown. In the middle, the geometric structure of 3D data is emphasized, demonstrating the increasing complexity of privacy concerns in the three-dimensional space. The right side indicates potential privacy risks in real-time 3D environments.

generating adversarial examples[14, 21], and using traditional methods like differential privacy and homomorphic encryption[6, 30, 32].

For information replacing and removal, some studies[1, 8, 11, 16] have concentrated on protecting privacy-sensitive facial attributes while maintaining functionality for tasks such as detection and tracking. The techniques range from face replacement and blurring. However, these methods rely on adversarial training, which is computationally expensive.

Adversarial examples[14, 21] have been applied to mislead unauthorized classification models. The classical security methods differential privacy and homomorphic encryption[6, 30, 32] have also been applied to safeguard the privacy of visual data. However, these methods do not utilize keys that can enhance privacy protection ability and restore protected data to its original form.

Moreover, to the best of our knowledge, 3D point cloud privacy has not been defined and addressed yet. Different from 2D video/image privacy, which is mostly related to visual texture, 3D point cloud does not contain the texture structure as 2D video/images, as shown in Figure 1. How-

ever, the 3D point cloud contains 3D geometry-specific privacy information, which is very sensitive in different applications such as virtual reality, 3D printing systems, and 3D high-resolution maps in self-driving systems, which leads to potential privacy leakage in the current 3D point cloud computing system. To address this new problem, in this work, we firstly proposed the 3D point cloud privacy problem and designed a computation-efficient and recognition-friendly privacy protection framework which can also inevitably encrypts the 3D point clouds in latent space efficiently.

Our proposed 3D point cloud privacy protection framework supporting both point cloud classification and segmentation tasks is shown in Figure 2. We proposed a conditional flow-based generation framework that projected the 3D point cloud into a latent Gaussian mixture model (GMM) distribution space, where each category is mapped into a Gaussian component. We rotate the latent Gaussian Mixture Model (GMM) using randomly encrypted orthogonal matrices so that the decoded 3D point cloud appears different from the original unless the correct decryption method is applied. Since the Gaussian mixture model property will be maintained after rotation, we can easily train a classification model on the encrypted point cloud to support the classification task without decryption. To this end, even the user can easily perform the classification task without seeing the original 3D point cloud. Similarly, we also proposed training a conditional flow-based 3D point cloud generation model for the point cloud segmentation task, as shown in (b). Each part of the 3D point cloud is mapped into a latent Gaussian mixture space with the same orthogonal rotation to encrypt the data. The user can also perform the segmentation task on the encrypted point cloud without seeing the original point cloud. Due to the computational cost of training the 3D point cloud generation model, we also designed an efficient, simplified single-flow model with angular similarity loss and empirically showed that we could achieve excellent results with fewer computational resources.

We summarize our contributions as follows:

- To the best knowledge, we are the first one who studied and solved the 3D point cloud privacy problem. Unlike 2D image privacy, which involves both texture and geometric structure, 3D point cloud privacy focuses solely on protecting the geometric structure.
- We proposed a flow-based generative model based 3D point cloud privacy protection method by projecting 3D point cloud into Gaussian Mixture Model latent space and rotating the latent space orthographically for privacy encryption. Since after rotation, the latent space distribution is unchanged, it encrypted point cloud can still be used to support 3D point cloud classification and segmentation tasks.
- We further proposed a angular similarity loss to reduce the number of flow-based generative model parameters, Our model achieves comparable performance to the original multiple-flow-based model using only a single-flow-based model. The training model size is reduced from 767Mb to 120Mb without reduction in performance. This enable the application of our model on low computational resources and improved the inference efficiency.
- We validate our approach through extensive experiments on synthetic and real-world datasets. The experimental results demonstrate the broad applicability and effectiveness of our approach.

## 2. Related work

### 2.1. 2D image video privacy protection

Up to now, 2D image and video privacy have been extensively researched within the field of computer vision. [22] was among the first to define data privacy, including considerations for 2D images and videos, with a focus on privacy-sensitive attributes such as faces. Building on this, numerous studies have explored approaches. Recent work [1, 8, 11, 16] has particularly concentrated on protecting sensitive facial attributes while maintaining the usefulness of the images for tasks like detection and tracking. [16] employs Conditional Generative Adversarial Networks (CGAN) to generate synthetic faces based on a specified identity, whereas [1] utilizes Style Generative Adversarial Networks (StyleGAN) to produce synthetic faces with a desired style. There is a password-based method [8] that enables anonymization and deanonymization using a password. In contrast to facial feature replacement, [11] directly blurs facial features while ensuring that the blurred features remain detectable by face detection models. In addition to facial features privacy protection, [3] focuses on preserving action-related attributes while protecting other sensitive information across video frames. Adversarial examples [14, 21] have been generated using various models to protect privacy in images, while [6] proposed a differential privacy method that pixelates images to enhance privacy, albeit without deep learning. Another approach, [30], achieves differential privacy by adding noise to an image’s feature vectors. Lastly, [32] introduced a homomorphic encryption system to protect visual data privacy. In summary, there are numerous methods available to safeguard the privacy of 2D data while preserving certain aspects of its usability. However, none of these methods are computationally efficient or provide keys( passwords) to restore the protected data to its original form.

### 2.2. 3D point cloud privacy protection

There are several methods available for protecting sensitive information in 2D images or videos, which can be

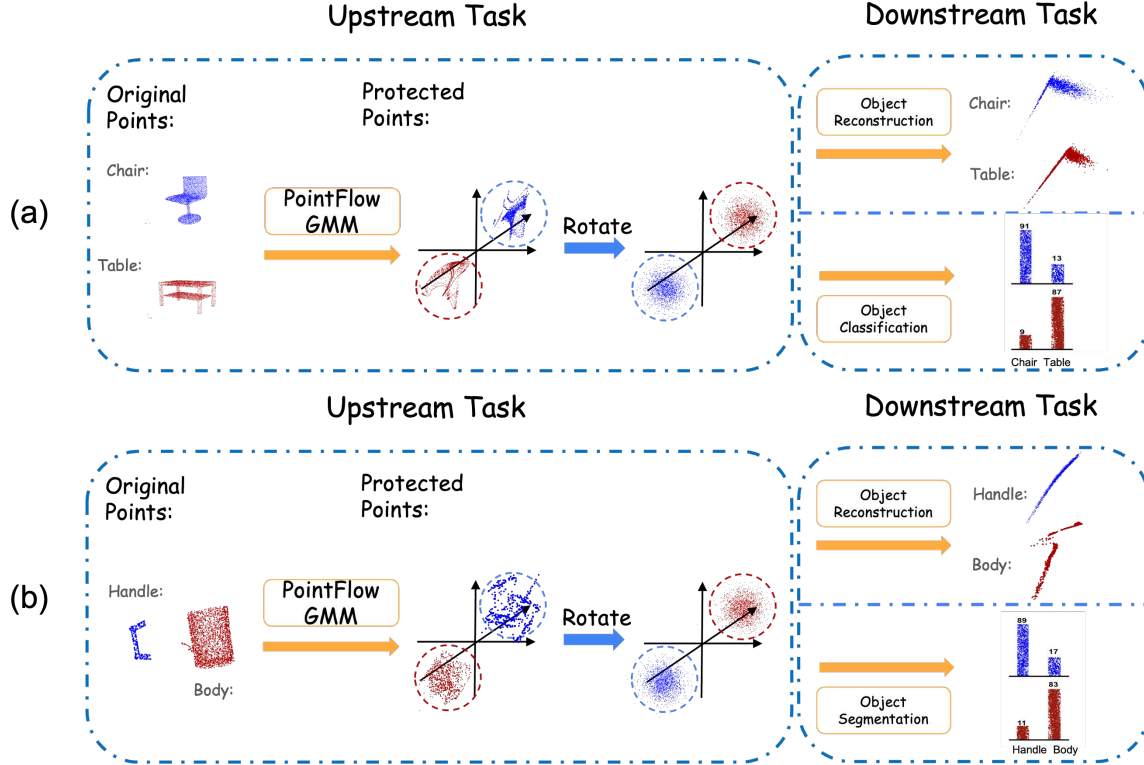


Figure 2. The privacy-preserving framework for 3D point cloud data addresses both recognition tasks and reconstruction suppression. (a) represents privacy protection for classification tasks, where the downstream task involves classifying the entire object. (b) illustrates privacy protection for segmentation tasks, where the downstream task focuses on segmenting individual points within a specific object or scene.

applied in different scenarios. Similarly, privacy protection for 3D data can be achieved using approaches analogous to those used for 2D data. [24] proposed a method to protect sensitive facial features from being reconstructed into original facial images while maintaining downstream classification performance. In [1, 16], the original face is replaced with a synthetic face to preserve detectability. Meanwhile, [11] employs a blurring technique using three types of loss functions to retain detection capabilities. Similarly, for protecting 3D geometric structure, the goal is to safeguard privacy while maintaining performance in downstream computer vision tasks. In this case, FlowGMM [10] effectively disrupts the geometric structure of point clouds while preserving the class information of the protected point clouds. Unlike GAN-based models, the flow-based generation model requires less computational resources during training. At this point, we devised angular similarity loss integrated with single flow to further reduce computation and storage costs. [7] proposed replacing faces with different “passwords,” where each password corresponds to a unique face style. With the correct password and reconstruction model, the original face can be restored. Therefore, for 3D geometric structure privacy, we can also develop a method

that reversibly protects its privacy. A simple key-based 2D image privacy protection method was proposed in [26]. A similar approach can be adapted for privacy protection in 3D point clouds.

### 3. Method

Let’s denote a 3D point cloud as  $\mathbf{X} = \{\mathbf{x}_i\}_{i=1}^n$ , where  $n$  is the number of points and  $\mathbf{y} \in \mathbb{R}^{C \times 1}$ ,  $C$  is the class number,  $\mathbf{Z} = \{\mathbf{z}_i\}_{i=1}^n$  is the point cloud in latent space. A Gaussian component in latent space is  $N(\mu, \sigma)$  where  $\mu$  and  $\sigma$  are mean and covariance. We first developed a framework comprising three main components, as shown in Figure 3. The Shape Representation Component (SRC) extracts shape features. The Point Transformation Component (PTC) then transforms individual points from a specific point cloud in the original space to points in the Gaussian mixture space, using shape features as conditional inputs. Finally, the Rotation Component (RC) rotates the points within the Gaussian mixture space.

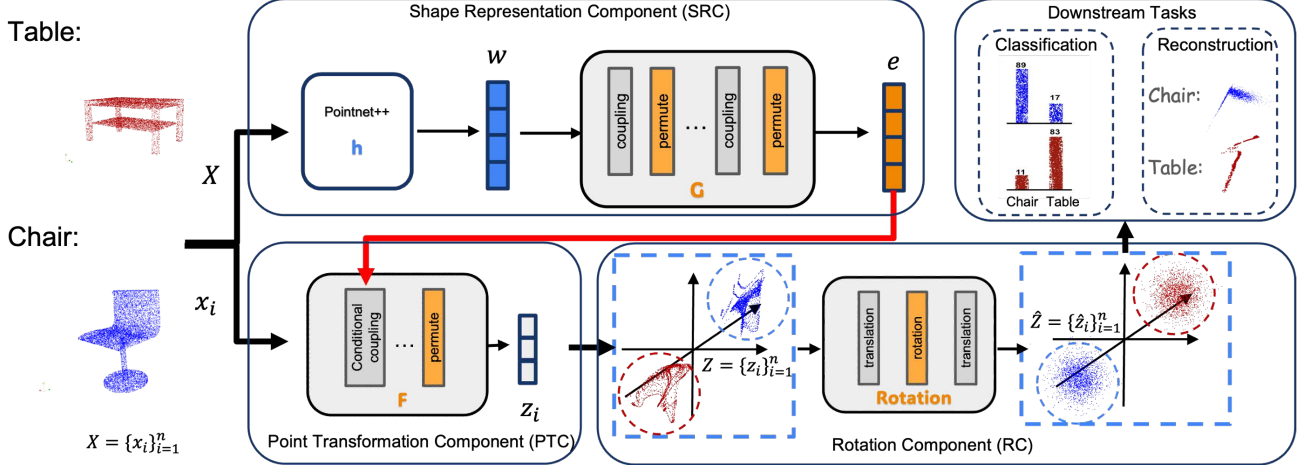


Figure 3. Pipeline for the PointFlowGMM model. The Gaussian Mixture Model in the latent space is predefined by assigning distinct means to each Gaussian component, with the covariance matrix set as the identity matrix. Note: The privacy protection process for classification and segmentation tasks follows the same pipeline; therefore, we choose to present the classification task as an example.

### 3.1. Shape Representation Component (SRC) and Point Transformation Component (PTC)

As shown in Figure 3, the Shape representation module consists of two parts: PointNet++[19] and FlowGMM[10]. PointNet++ is used to extract the shape features of the original point cloud data. The extracted shape features have a non-linear decision boundary. To address this, we use FlowGMM to transform these shape features into a Gaussian mixture space with a linear decision boundary, which significantly facilitates the training process for the Point Transformation Component (PTC). The formula of SRC can be expressed as follows:

$$e = G(w), \quad w = h(X). \quad (1)$$

Herein,  $h$  is a function of the PointNet++ to extract shape feature vector  $w \in \mathbb{R}^{1 \times m}$  from a sample of the point cloud  $X$ , where  $m$  is a pre-defined parameter denoting dimension of the shape feature vector.  $w$  will be passed through the encoder  $G$  of a FlowGMM model to form the shape representation  $e \in \mathbb{R}^{1 \times m}$ , which is a latent shape vector following a Gaussian mixture distribution.

The Point Transformation Component primarily uses a FlowGMM with an additional conditional input[17]. Unlike a standard FlowGMM that takes a single input, PTC receives an additional input as a condition. PTC takes the 3D coordinates of an individual point within a point cloud (local feature) and the shape feature of the entire point cloud as inputs. This approach is essential to ensure that our framework can be applied to both classification and segmentation tasks. For classification, using the shape feature as a condition ensures that points from different shapes are assigned to distinct Gaussian components. For segmentation,

the unique coordinates of each point ensure that points belonging to different parts are assigned to different Gaussian components. Projecting the original point clouds to Gaussian-distributed point clouds offers an important advantage. This projection disrupts the geometric structure of the original point clouds while retaining class information by assigning point clouds from different parts or shapes to distinct Gaussian components with unique means. The formula of PTC and its inverse can be expressed as follows:

$$z_i = F(x_i, e), \quad x_i = F^{-1}(z_i, e) \quad (2)$$

where  $F$  is the function of a FlowGMM model with a conditional input,  $z_i \in Z$  follows a Gaussian mixture distribution, and  $x_i \in X$  follows the original distribution.

### 3.2. Rotation Component (RC) and Reconstruction

To strengthen the privacy protection of our proposed model, two orthogonal rotation matrices are employed to rotate points in latent space. The first matrix is used for rotating individual points within a specific Gaussian component, referred to as point rotation. Point rotation, utilizing the rotation method from [26], not only enhances privacy protection but also ensures that the rotated points are perfectly distributed within a specific Gaussian component. As illustrated in Figure 3, the red and blue point clouds are perfectly distributed in space after RC. The second matrix is applied to rotate the centers of the Gaussian components within the entire Gaussian mixture space, referred to as center rotation. For point rotation, a translation matrix  $T_1$  calculated by the mean of a point cloud in latent space is used to translate the point cloud  $Z$  to the origin in the 3D coordinate system. The translated point cloud,  $Z - T_1$ , is then multiplied by a common point rotation matrix  $R_p$ , result-

ing in  $(Z - T_1)R_p$ . Next, for center rotation, the original translation matrix is multiplied by a specific center rotation matrix  $R_c$ , yielding

$$T_2 = T_1 R_c \quad (3)$$

which translates the rotated center to its new position. Thus, the final rotated point cloud is given by

$$\hat{Z} = (Z - T_1)R_p + T_2 \quad (4)$$

Applying the same rotation operation to other points in the entire or a part of the point cloud ensures consistent protection. Due to the rotation invariance of the Gaussian distribution, the rotated point cloud  $\hat{Z}$  still preserves category information.

The original data can be reconstructed by

$$Z = (\hat{Z} - T_2 R_c^T) R_p^T + T_2 R_c^T \quad (5)$$

$$X = F^{-1}(Z|e) \quad (6)$$

where  $T_2$  is calculated by the mean of the point clouds in rotated latent space. Hence, one that has the correct key  $R_c$ ,  $R_p$ , and the inverse of the conditional FlowGMM models used can recover the original point cloud from the protected point cloud.

### 3.3. Loss Functions for Training

For the training loss, the points in the point cloud of a specific category will be transformed to the Gaussian component  $k$  corresponding to that category. So, the loss functions for SRC and PTC are both negative log-likelihoods:

$$L_{nll} = -\log p_{\mathcal{X}}(\mathbf{x}|y = k) \quad (7)$$

For SRC, according to change of variable formula, its specific loss function is:

$$\begin{aligned} L_s &= -\log p_{\mathcal{X}}(X|y = k_s) \\ &= -\log N(G(\mathbf{w})|\boldsymbol{\mu}_{k_s}^e, \boldsymbol{\Sigma}_{k_s}^e) - \log \left| \det\left(\frac{\partial G}{\partial \mathbf{w}}\right) \right| \end{aligned} \quad (8)$$

where  $k_s$  is the shape label.

For PTC, according to change of variable formula, its specific loss function is:

$$\begin{aligned} L_p^i &= -\log p_{x_i}(\mathbf{x}_i|y = k_p) \\ &= -\log N(F(\mathbf{x}_i, \mathbf{e})|\boldsymbol{\mu}_{k_p}^z, \boldsymbol{\Sigma}_{k_p}^z) - \log \left| \det\left(\frac{\partial F}{\partial \mathbf{x}_i}\right) \right|, \end{aligned} \quad (9)$$

where  $k_p$  represents a point-wise label.

To ensure privacy protection, points in the latent space should appear distinct from those in the original space.

Therefore, a loss function is required to encourage a random shift of points in the latent space. We introduce the angular similarity loss that shifts the points in the latent space away from their original counterparts. To make the original points comparable with the latent points, we calculate the vectors relative to their respective centers ( $\boldsymbol{\mu}_{k_p}^x$  and  $\boldsymbol{\mu}_{k_p}^z$  respectively).

$$V_o^i = \mathbf{x}_i - \boldsymbol{\mu}_{k_p}^x \quad (10)$$

$$V_l^i = \mathbf{z}_i - \boldsymbol{\mu}_{k_p}^z \quad (11)$$

where  $V_o$  and  $V_l$  represents vectors in original and latent space for point  $i$ .

This allows us to use cosine similarity to compare these two vectors. For each point  $i$ , a shift  $\beta$  is sampled from a uniform distribution  $[-1,1]$  to determine its displacement from the original space. The resulting loss function is as follows:

$$L_{as}^i = |\text{Cosine}(V_o^i, V_l^i) - \beta| \quad (12)$$

where  $\text{Cosine}(\cdot)$  calculates the cosine similarity between two vectors.

The angular similarity loss also enables us to reduce the number of flows in FlowGMM, as our goal is to map points with different shapes or parts to different Gaussian components rather than extracting more abstract features. For PTC, we use only a single flow, which significantly reduces computation and storage requirements. However, this approach preserves the geometric structure of point clouds in the latent space. In this case, the angular similarity loss achieves random displacement between points in the original space and their corresponding points in the latent space. When angular similarity loss is added during the training process, the geometric structure of point clouds in the latent space can become further disrupted. This will be discussed further in Section 3.4. Overall, the angular similarity loss not only enhances the privacy protection ability of PTC but also conserves substantial computation and storage resources.

The final loss function is:

$$L = \lambda_s \cdot L_s + \lambda_p \cdot \sum_{i=1}^n L_p^i + \lambda_{as} \cdot \sum_{i=1}^n L_{as}^i \quad (13)$$

These two FlowGMM models are trained together, and thus  $G$  and  $F$  are obtained simultaneously after the training process to compose the PointFlowGMM framework.

### 3.4. With/Without Angular Similarity Loss Comparison

Angular similarity loss plays a key role in our method. Since our goal is to obscure the geometric structure of the original point clouds, it is not necessary to use multiple flows for precise point transformation, as this would require substantial computational resources. Instead, angular

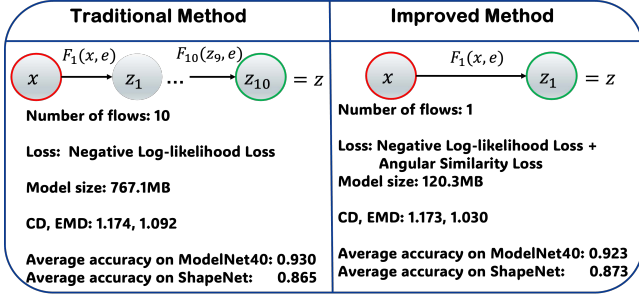


Figure 4. Comparison diagram: The left side shows the architecture with multiple flows, while the right side displays the architecture with a single flow.

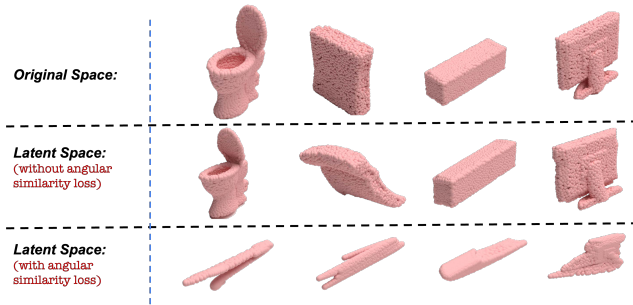


Figure 5. A comparative study on the impact of adding angular similarity loss to PTC(a single flow).

similarity loss effectively disrupts the geometric structure of point clouds in the original space. Therefore, we use a single flow with angular similarity loss to achieve comparable obfuscation and downstream recognition results while reducing computation and storage requirements, as shown in Figure 4. More experiment results are shown in the Supplementary Material. Furthermore, to demonstrate its effectiveness, we conduct a comparison study on this loss using only a single flow for the PTC. As shown in Figure 5, when angular similarity loss is omitted, the transformations of point clouds in the latent space are minimal. However, with angular similarity loss, the transformed point clouds become nearly unrecognizable to the human eye.

## 4. Experiments

In this section, we first run simulations to demonstrate the effectiveness of the proposed model in preserving privacy and then conduct proof-of-concept classification and segmentation experiments to prove data usability of the point clouds after transformation and rotation.

### 4.1. Model Settings and Datasets

We used the RealNVP [5] architecture to train our FlowGMM models, where  $G$  utilizes two coupling layers

and  $F$  employs one conditional coupling layer. The neural network within the coupling layer is based on DenseNet, with each hidden layer containing 512 neurons. For SRC, we used the PointNet++ [19] feature extractor to obtain the shape feature  $w$ , setting the shape representation dimension  $\hat{e}$  to  $m = 32$ . The size of each point cloud is set to  $n = 2048$  after applying the farthest point sampling. Before training FlowGMM, we sampled the means  $\mu_k^e$  and  $\mu_k^z$  from their respective Gaussian distributions, ensuring maximum separation between the means  $\mu_k^e$  and  $\mu_k^z$  for each class  $k$ . The variance  $\Sigma_k$  of each Gaussian distribution is fixed to the identity matrix  $I_m$ . All experiments were conducted on one NVIDIA RTX A6000 GPUs.

We used the following datasets for our proof-of-concept experiments: **ModelNet** [28]: A widely-used dataset for 3D model classification, containing over 127,915 hand-drawn CAD point cloud models. ModelNet10 and ModelNet40 are popular subsets, covering 10 and 40 categories, respectively, for point cloud classification tasks. **ShapeNet** [2]: A large collection of synthetic CAD models widely used in classification and segmentation tasks. It includes 16 main categories, with each point labeled within these categories, yielding 55 subcategories. ShapeNet was used in our experiments to evaluate the performance of encrypted point clouds in segmentation tasks, demonstrating data usability. **ScanObjectNN** [23]: A realistic point cloud dataset frequently used for classification tasks, containing 2,902 3D objects across 15 categories derived from indoor scans. This dataset, based on real-world scenes, presents a greater challenge compared to CAD-based point clouds.

### 4.2. Privacy-Preserving Ability

We firstly assess the privacy-preserving capability of our method on point clouds. Since all transformed point clouds are mapped into their Gaussian space, they no longer resemble the original shapes of human vision. To quantify privacy protection, we calculate the similarity between the original and protected point clouds: the lower the similarity score, the stronger the privacy protection. Following prior work [27, 31], we use Chamfer Distance (CD) and Earth Mover’s Distance (EMD) as metrics for the similarity between the original and protected point clouds. Lower CD/EMD scores indicate higher similarity; thus, higher scores indicate stronger privacy protection. We compare our method to Differential Privacy (DP) techniques, applying Laplacian noise at various strengths, with  $\epsilon \in [0.5, 10]$ . As shown in Table 1, our protected point clouds yield higher CD and EMD scores than DP, indicating lower similarity to the original data. To further evaluate our method’s resistance to computer vision attacks, we trained a PointNet++ classifier on the original ModelNet10 point clouds to recognize different classes, as summarized in Table 1. ”Accuracy overall” represents the proportion of correctly classi-

Table 1. CD scores and EMD scores between the original point cloud and protected point cloud.

	CD	EMD	Accuracy overall	Accuracy avg.class
original	0	0	0.9317	0.9240
$\epsilon = 10$	0.0702	0.0455	0.4670	0.4120
$\epsilon = 5$	0.1037	0.0731	0.1608	0.151
$\epsilon = 1$	0.4321	0.4018	0.1178	0.113
$\epsilon = 0.5$	1.0271	1.0002	0.1112	0.109
protected	1.1738	1.0304	0.1057	0.0853

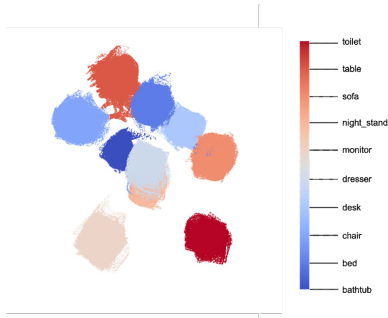


Figure 6. Points in latent space, each color represents a class.

fied samples out of the total, while "Accuracy avg. class" is the average accuracy across categories. Results indicate that classification accuracy on the protected point clouds was around 10%, meaning our method effectively prevents unauthorized recognition.

### 4.3. Class information-Preserving Ability

As shown in Figure 6, our method maps points from the original 3D space of the ModelNet10 dataset into a Gaussian mixture latent space, where points from different categories correspond to distinct Gaussian distributions. This separation preserves category information, creating identifiable clusters for each class. Even when the original 3D geometry is hidden, category distinctions remain, enabling the transformed point clouds to support downstream tasks.

### 4.4. The Classification Tasks

In this part, we validate the data usability of the protected point cloud generated by our method. We used the ModelNet and ScanObjectNN datasets for our classification tasks. Training and testing sets are split in the same way as described in [18, 23, 28]. We first trained the PointFlowGMM model on the training set of ModelNet and ScanObjectNN. Then, the whole original dataset will go through the PointFlowGMM model to result in the protected point clouds. We specifically used MLP as the classifier, which is trained on the training set of the protected point cloud. Note that

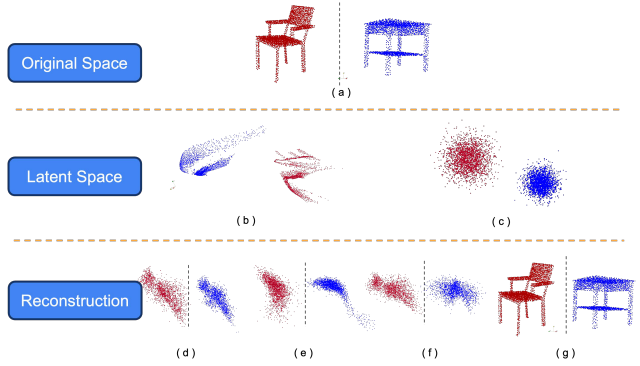


Figure 7. Transformation and reconstruction: (a) the original point cloud, (b) the latent point cloud, (c) the latent point cloud after rotation, (d) wrong  $R_c$  and wrong  $R_p$ , (e) correct  $R_c$  and wrong  $R_p$ , (f) wrong  $R_c$  and correct  $R_p$ , (g) correct  $R_c$  and correct  $R_p$ .

Table 2. Comparison of classification accuracy.

Dataset	Model	Point cloud	Accuracy overall	Accuracy avg.class
ModelNet10	PointNet++	original	0.9317	0.9228
	MLP	protected	0.9228	0.9017
ModelNet40	PointNet++	original	0.9036	0.8660
	MLP	protected	0.8968	0.8673
Scan ObjectNN	PointNet++	original	0.8554	0.8211
	MLP	protected	0.8107	0.7811

the classifier for original point clouds is PointNet++ [19] trained on the original ModelNet and ScanObjectNN training set. Each classifier is trained for 20 epochs. Table 2 shows that the classification accuracies of the protected point clouds are comparable to (slightly worse than) the original point clouds. This shows that the protected point clouds preserve data usability for downstream classification tasks.

Then we set up experiments to show that our privacy-preserving method is invertible. Figure 7 (a) shows an original point cloud of an airplane. Through SRC and PTC, it is transformed into a latent point cloud in the latent space, as shown in Figure 7 (b). We then rotated the point cloud with the keys  $R_c$  and  $R_p$  to obtain the protected point cloud in Figure 7 (c). We will reconstruct the wrong point cloud using the wrong keys as shown in Figure 7 (d), (e), and (f). By utilizing the correct keys  $R_c$  and  $R_p$ , we can recover the original point cloud as shown in Figure 7 (g).

### 4.5. The Segmentation Tasks

We further validated the effectiveness of our proposed privacy-preserving method for data usability on the

Table 3. Segmentation results on ShapeNet parts dataset. The evaluation metric is accuracy(%) on points. We compare the original point cloud with the protected point cloud.

	mean	aero	bag	cap	car	chair	ear phone	guitar	knife	lamp	laptop	motor	mug	pistol	rocket	skate board	table
shapes		2690	76	55	898	3758	69	787	392	1547	451	202	184	283	66	152	5271
original	89.2	87.2	90.9	70.5	85.3	91.3	74.5	93.7	89.2	86.4	93.4	77.4	96.3	92.6	73.3	90.7	89.7
protected	87.3	86.2	92.0	83.5	83.2	88.1	77.2	90.4	92.3	82.5	87.6	72.0	90.6	90.2	82.2	88.8	89.2

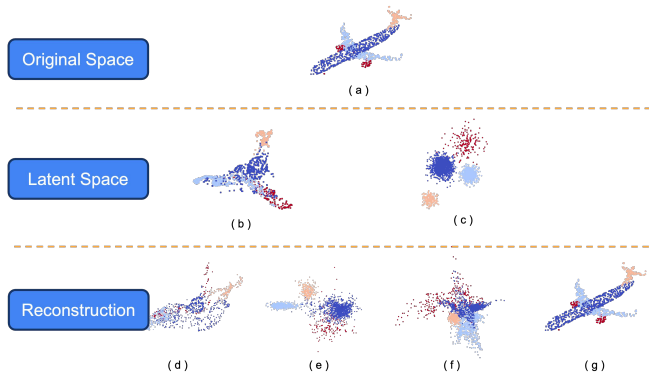


Figure 8. Transformation and reconstruction for segmentation task: (a) the original point cloud, (b) the latent point cloud, (c) the latent point cloud after rotation, (d) incorrect  $R_c$  and  $R_p$ , (e) incorrect  $R_c$  and correct  $R_p$ , (f) correct  $R_c$  and incorrect  $R_p$ , (g) point cloud reconstructed with both correct keys.

ShapeNet dataset, specifically for segmentation tasks. We partitioned the dataset into training and testing sets following the same approach as in [2, 18]. PointFlowGMM models were trained similarly to previous classification tasks, and we then applied PointNet [18] and an MLP model on the original and protected point clouds, respectively, for the segmentation task, training each model for 20 epochs.

Table 3 shows that our protected point clouds achieve successful segmentation, with only a 1.9% decrease in accuracy compared to the original point clouds. This demonstrates that our privacy-preserving method maintains data usability while protecting the privacy of point cloud information. Additionally, we observe in Table 3 that classes with a larger number of point clouds (e.g., chairs and tables) show minimal accuracy deterioration, whereas classes with fewer instances (e.g., bags, hats, and headphones) exhibit a more noticeable drop in accuracy. This may result from an imbalance in class distribution within the Gaussian space, affecting the effectiveness of segmentation for less-represented categories.

In Figure 8, we illustrate the segmentation task on a protected point cloud and visualize the reconstructed segmentation outcomes. Figures 8 (b) and (c) demonstrate that the Rotation Component effectively distributes points across

different segments within the latent space, preserving both category information and the Gaussian mixture distribution. In Figures 8 (d), (e), and (f), it is evident that without the proper reconstruction method (both  $R_c$  and  $R_p$  are correct), the original point cloud cannot be accurately recovered. 8 (g) shows that if both rotation matrices  $R_c$  and  $R_p$  are correct, the original point cloud can be recovered in the segmentation task.

## 5. Conclusion

With the increasing use of 3D point clouds across various applications, privacy concerns regarding the geometric structure of 3D point cloud data have become evident. While numerous privacy protection methods exist for different types of 2D data, such as images and videos, there has been limited focus on protecting the privacy of 3D point clouds. To address this gap, we proposed an efficient method that leverages elements from 2D privacy protection techniques to safeguard 3D point cloud data. Many 2D privacy protection approaches retain the usability of protected data for downstream tasks, such as allowing protected face images for detection or tracking. However, these methods are often computationally intensive or lack support for key-based recovery to restore protected data to its original form. Our approach utilizes FlowGMM with a single flow and angular similarity loss to reduce computational overhead. To ensure the proposed method is applicable for both classification and segmentation tasks, we incorporate the Shape Representation Component (SRC) and Point Transformation Component (PTC) to capture global shape and local point features, respectively. Additionally, to support key-based recovery and enhance privacy protection, we introduce a Rotation Component (RC) that rotates point clouds within the latent space. Finally, we validate our method through experiments on various public datasets, demonstrating its promising performance.

## References

- [1] Simone Barattin, Christos Tzelepis, Ioannis Patras, and Nicu Sebe. Attribute-preserving face dataset anonymization via latent code optimization. In *Proceedings of the IEEE/CVF conference on computer vision and pattern recognition*, pages 8001–8010, 2023. 1, 2, 3
- [2] Angel X. Chang, Thomas Funkhouser, Leonidas Guibas, Pat Hanrahan, Qixing Huang, Zimo Li, Silvio Savarese, Manolis Savva, Shuran Song, Hao Su, Jianxiong Xiao, Li Yi, and Fisher Yu. ShapeNet: An Information-Rich 3D Model Repository, 2015. 6, 8
- [3] Ishan Rajendrakumar Dave, Chen Chen, and Mubarak Shah. Spact: Self-supervised privacy preservation for action recognition. In *Proceedings of the IEEE/CVF Conference on Computer Vision and Pattern Recognition*, pages 20164–20173, 2022. 1, 2
- [4] Jaybie A de Guzman, Kanchana Thilakarathna, and Aruna Seneviratne. A first look into privacy leakage in 3d mixed reality data. In *Computer Security—ESORICS 2019: 24th European Symposium on Research in Computer Security, Luxembourg, September 23–27, 2019, Proceedings, Part I 24*, pages 149–169. Springer, 2019. 1
- [5] Laurent Dinh, Jascha Sohl-Dickstein, and Samy Bengio. Density estimation using Real NVP. In *International Conference on Learning Representations*, 2017. 6
- [6] Liyue Fan. Image pixelization with differential privacy. In *Data and Applications Security and Privacy XXXII: 32nd Annual IFIP WG 11.3 Conference, DBSec 2018, Bergamo, Italy, July 16–18, 2018, Proceedings 32*, pages 148–162. Springer, 2018. 1, 2
- [7] Xiuye Gu, Weixin Luo, Michael S Ryoo, and Yong Jae Lee. Password-conditioned anonymization and deanonymization with face identity transformers. In *European conference on computer vision*, pages 727–743. Springer, 2020. 3
- [8] Xiuye Gu, Weixin Luo, Michael S Ryoo, and Yong Jae Lee. Password-conditioned anonymization and deanonymization with face identity transformers. In *European conference on computer vision*, pages 727–743. Springer, 2020. 1, 2
- [9] Jaybie Agullo de Guzman, Aruna Seneviratne, and Kanchana Thilakarathna. Unravelling spatial privacy risks of mobile mixed reality data. *Proceedings of the ACM on Interactive, Mobile, Wearable and Ubiquitous Technologies*, 5(1):1–26, 2021. 1
- [10] Pavel Izmailov, Polina Kirichenko, Marc Finzi, and Andrew Gordon Wilson. Semi-Supervised Learning with Normalizing Flows. In *Proceedings of the 37th International Conference on Machine Learning*, pages 4615–4630. PMLR, 2020. 3, 4
- [11] Baowei Jiang, Bing Bai, Haozhe Lin, Yu Wang, Yuchen Guo, and Lu Fang. Dartblur: Privacy preservation with detection artifact suppression. In *Proceedings of the IEEE/CVF Conference on Computer Vision and Pattern Recognition*, pages 16479–16488, 2023. 1, 2, 3
- [12] Hyunoh Lee, Jinwon Lee, Hyungki Kim, and Duhwan Mun. Dataset and method for deep learning-based reconstruction of 3D CAD models containing machining features for mechanical parts. *Journal of Computational Design and Engineering*, 9(1):114–127, 2022. 1
- [13] Wen Li, Shangshu Yu, Cheng Wang, Guosheng Hu, Siqi Shen, and Chenglu Wen. SGLoc: Scene Geometry Encoding for Outdoor LiDAR Localization. In *Proceedings of the IEEE/CVF Conference on Computer Vision and Pattern Recognition*, pages 9286–9295, 2023. 1
- [14] Jiang Liu, Chun Pong Lau, and Rama Chellappa. Diff-protect: Generate adversarial examples with diffusion models for facial privacy protection. *arXiv preprint arXiv:2305.13625*, 2023. 1, 2
- [15] Lingfei Ma, Ying Li, Jonathan Li, Yongtao Yu, José Marcato Junior, Wesley Nunes Gonçalves, and Michael A Chapman. Capsule-based networks for road marking extraction and classification from mobile LiDAR point clouds. *IEEE Transactions on Intelligent Transportation Systems*, 22(4):1981–1995, 2020. 1
- [16] Maxim Maximov, Ismail Elezi, and Laura Leal-Taixé. Ciagan: Conditional identity anonymization generative adversarial networks. In *Proceedings of the IEEE/CVF conference on computer vision and pattern recognition*, pages 5447–5456, 2020. 1, 2, 3
- [17] Albert Pumarola, Stefan Popov, Francesc Moreno-Noguer, and Vittorio Ferrari. C-Flow: Conditional Generative Flow Models for Images and 3D Point Clouds. In *Proceedings of the IEEE/CVF Conference on Computer Vision and Pattern Recognition (CVPR)*, 2020. 4
- [18] Charles R. Qi, Hao Su, Kaichun Mo, and Leonidas J. Guibas. PointNet: Deep Learning on Point Sets for 3D Classification and Segmentation. In *Proceedings of the IEEE Conference on Computer Vision and Pattern Recognition (CVPR)*, 2017. 7, 8
- [19] Charles Ruizhongtai Qi, Li Yi, Hao Su, and Leonidas J Guibas. PointNet++: Deep Hierarchical Feature Learning on Point Sets in a Metric Space. In *Advances in Neural Information Processing Systems*. Curran Associates, Inc., 2017. 4, 6, 7
- [20] Thinal Raj, Fazida Hanim Hashim, Aqilah Baseri Huddin, Mohd Faisal Ibrahim, and Aini Hussain. A survey on LiDAR scanning mechanisms. *Electronics*, 9(5):741, 2020. 1
- [21] Fahad Shamshad, Muzammal Naseer, and Karthik Nandakumar. Clip2protect: Protecting facial privacy using text-guided makeup via adversarial latent search. In *Proceedings of the IEEE/CVF Conference on Computer Vision and Pattern Recognition*, pages 20595–20605, 2023. 1, 2
- [22] Latanya Sweeney. k-anonymity: A model for protecting privacy. *International journal of uncertainty, fuzziness and knowledge-based systems*, 10(05):557–570, 2002. 2
- [23] Mikaela Angelina Uy, Quang-Hieu Pham, Binh-Son Hua, Thanh Nguyen, and Sai-Kit Yeung. Revisiting Point Cloud Classification: A New Benchmark Dataset and Classification Model on Real-World Data. In *Proceedings of the IEEE/CVF International Conference on Computer Vision (ICCV)*, 2019. 6, 7
- [24] Zhibo Wang, He Wang, Shuaifan Jin, Wenwen Zhang, Jiahui Hu, Yan Wang, Peng Sun, Wei Yuan, Kaixin Liu, and Kui Ren. Privacy-preserving adversarial facial features. In *Pro-*

- ceedings of the IEEE/CVF Conference on Computer Vision and Pattern Recognition*, pages 8212–8221, 2023. 3
- [25] Chenglu Wen, Xiaotian Sun, Jonathan Li, Cheng Wang, Yan Guo, and Ayman Habib. A deep learning framework for road marking extraction, classification and completion from mobile laser scanning point clouds. *ISPRS journal of photogrammetry and remote sensing*, 147:178–192, 2019. 1
- [26] Chenwei Wu, Chenzhuang Du, and Yang Yuan. Secure Data Sharing With Flow Model, 2020. 3, 4
- [27] Tong Wu, Liang Pan, Junzhe Zhang, Tai Wang, Ziwei Liu, and Dahua Lin. Density-aware chamfer distance as a comprehensive metric for point cloud completion. *arXiv preprint arXiv:2111.12702*, 2021. 6
- [28] Zhirong Wu, Shuran Song, Aditya Khosla, Fisher Yu, Linguang Zhang, Xiaoou Tang, and Jianxiong Xiao. 3D ShapeNets: A Deep Representation for Volumetric Shapes. In *Proceedings of the IEEE Conference on Computer Vision and Pattern Recognition (CVPR)*, 2015. 1, 6, 7
- [29] Zhennan Wu, Yang Li, Yifei Huang, Lin Gu, Tatsuya Harada, and Hiroyuki Sato. 3D Segmenter: 3D Transformer based Semantic Segmentation via 2D Panoramic Distillation. In *The Eleventh International Conference on Learning Representations*, 2022. 1
- [30] Hanyu Xue, Bo Liu, Ming Ding, Tianqing Zhu, Dayong Ye, Li Song, and Wanlei Zhou. Dp-image: Differential privacy for image data in feature space. *arXiv preprint arXiv:2103.07073*, 2021. 1, 2
- [31] Guandao Yang, Xun Huang, Zekun Hao, Ming-Yu Liu, Serge Belongie, and Bharath Hariharan. PointFlow: 3D Point Cloud Generation With Continuous Normalizing Flows. In *Proceedings of the IEEE/CVF International Conference on Computer Vision (ICCV)*, 2019. 6
- [32] Ryo Yonetani, Vishnu Naresh Boddeti, Kris M Kitani, and Yoichi Sato. Privacy-preserving visual learning using doubly permuted homomorphic encryption. In *Proceedings of the IEEE international conference on computer vision*, pages 2040–2050, 2017. 1, 2
- [33] Jinghuai Zhang, Jinyuan Jia, Hongbin Liu, and Neil Zhenqiang Gong. PointCert: Point Cloud Classification with Deterministic Certified Robustness Guarantees. In *Proceedings of the IEEE/CVF Conference on Computer Vision and Pattern Recognition*, pages 9496–9505, 2023. 1